Blood Cancer Journal www.nature.com/bcj

ARTICLE OPEN

Check for updates

MYC-rearranged mature B-cell lymphomas in children and young adults are molecularly Burkitt Lymphoma

Sara Mato[1,2,15], Natalia Castrejón-de-Anta[2,3,15], Ariadna Colmenero[1,2,15], Lorenzo Carità[1], Julia Salmerón-Villalobos[1], Joan Enric Ramis-Zaldivar[1,4], Ferran Nadeu[1,4], Noelia Garcia[1], Luojun Wang[3], Jaime Verdú-Amorós[4,5], Mara Andrés[6], Nuria Conde[7], Verónica Celis[7], Maria José Ortega[8], Ana Galera[9], Itziar Astigarraga[10], Vanesa Perez-Alonso[11], Eduardo Quiroga[12], Aixiang Jiang[13], David W. Scott[13,14], Elias Campo[1,2,3,4], Olga Balagué[1,2,3,4,16]✉ and Itziar Salaverria[1,4,16]✉

Aggressive B-cell non-Hodgkin lymphomas (NHL) in children, adolescents, and young adults (CAYA) include Burkitt lymphoma (BL), diffuse large B-cell lymphoma (DLBCL), and a subset of high-grade tumors with features intermediate between these entities whose genetic and molecular profiles have not been completely elucidated. In this study, we have characterized 37 aggressive B-NHL in CAYA, 33 with high-grade morphology, and 4 DLBCL with *MYC* rearrangement (*MYC*-R), using targeted next-generation sequencing and the aggressive lymphoma gene expression germinal center B-cell-like (GCB), activated B-cell-like (ABC), and dark zone signatures (DZsig). Twenty-two tumors had *MYC*-R without *BCL2* breaks, and two *MYC*-non-R cases had *BCL6* translocations. *MYC*-R cases, including DLBCL, carried BL-related mutations and copy number alterations. Conversely, *MYC*-non-R lymphomas had alterations in the B-cell receptor signaling/NF-κB pathway (71%). DZsig was expressed in 12/13 of *MYC*-R tumors but only in 2/10 of *MYC*-non-R GCB tumors ($P < 0.001$). The 3-year event-free survival (EFS) of the whole cohort was 79.6%. *TP53* and *KMT2C* mutations conferred inferior outcome (3-year EFS $P < 0.05$). Overall, *MYC*-R lymphomas in CAYA have a molecular profile similar to BL regardless of their high-grade or DLBCL morphology, whereas *MYC*-non-R has more heterogeneous genetic alterations closer to that of DLBCL.

Blood Cancer Journal (2024)14:171 ; https://doi.org/10.1038/s41408-024-01153-0

INTRODUCTION

High-grade B-cell lymphoma, not otherwise specified (HGBCL, NOS) is a diagnostic category introduced in the revised 4th edition of the World Health Organization (WHO) classification of lymphoid malignancies [1] and maintained in current lymphoid neoplasms diagnostic guidelines [2, 3]. This diagnostic class emerged from the dissolution of the wide WHO 2008 category of B-cell lymphoma, unclassifiable, (BCLU) with features intermediate between diffuse large B-cell lymphoma (DLBCL) and Burkitt lymphoma (BL), which encompassed a heterogeneous subset of mature B-cell lymphomas with morphological appearances from blastoid to features intermediate between BL and DLBCL. The HGBCL, NOS category retains this morphological spectrum, in the lack of concomitant *MYC* and *BCL2* and/or *BCL6* rearrangements (HGBCL-Double hit [DH]), although 20–50% of them display *MYC* rearrangements (*MYC*-R) [2–4]. In adults, all HGBCL entities have very poor prognosis with a median overall survival of less than two years [4–6]. The genetic landscape of HGBCL, NOS is still poorly understood and up to date, only two different studies have highlighted the molecular heterogeneity of these tumors, describing an intermediate mutational profile between BL and DLBCL [7, 8]. Two independent studies have proposed gene expression signatures of poor outcomes to identify these patients [9, 10]. Both molecular high-grade (MHG) [9] and DH signatures (DHITsig) [10] are able to identify most of DH as well as a subset of non-DH and distinguish them from the relatively favorable germinal center B-cell-like (GCB) DLBCL. Moreover, DHITsig defines a group of aggressive GCB lymphomas that extend beyond HGBCL-DH and is also shared with archetypical dark zone lymphomas as BL, an aspect that motivated to rename it dark zone signature (DZsig) [11]. Recognition that a subset of non-DH tumors displays this DZsig raises the possibility that a proportion of HGBCL, NOS could harbor *MYC* or other relevant rearrangements that are cryptic to fluorescence in situ hybridization (FISH), as it has been previously

[1]Institut d'Investigacions Biomèdiques August Pi i Sunyer (IDIBAPS), Barcelona, Spain. [2]University of Barcelona (UB), Barcelona, Spain. [3]Hematopathology Section, Laboratory of Pathology, Hospital Clinic de Barcelona, Barcelona, Spain. [4]Centro de Investigación Biomédica en Red de Cáncer (CIBERONC), Madrid, Spain. [5]Pediatric Oncology Department, Hospital Clínico Universitario, Biomedical Research Institute INCLIVA de Valencia, Valencia, Spain. [6]Pediatric Oncology Department, Hospital La Fe, Valencia, Spain. [7]Pediatric Oncology Department, Hospital Sant Joan de Déu, Esplugues de Llobregat, Spain. [8]Pediatric Oncology Department, Hospital Virgen de las Nieves, Granada, Spain. [9]Pediatric Oncohematology Department, Hospital Clínico Universitario Virgen de la Arrixaca, Murcia, Spain. [10]Pediatric Oncology Unit, Hospital Universitario Cruces Osakidetza, Biocruces Bizkaia Health Research Institute, Barakaldo, Spain. [11]Pediatric Oncology Department, Hospital Universitario 12 de Octubre, Madrid, Spain. [12]Pediatric Oncology Department, Hospital Virgen del Rocio, Sevilla, Spain. [13]BC Cancer's Centre for Lymphoid, Vancouver, BC, Canada. [14]Division of Medical Oncology, Department of Medicine, University of British Columbia, Vancouver, BC, Canada. [15]These authors contributed equally: Sara Mato, Natalia Castrejón-de-Anta, Ariadna Colmenero. [16]These authors jointly supervised this work: Olga Balagué, Itziar Salaverria. ✉email: obalague@clinic.cat; isalaver@recerca.clinic.cat

Received: 24 July 2024 Revised: 20 September 2024 Accepted: 23 September 2024
Published online: 07 October 2024

observed in other lymphoma entities by next-generation sequencing (NGS) approaches [12–15].

In children and adolescents, BL and DLBCL are the predominant mature B-cell lymphomas. Although the revised 4th WHO classification [1] recommended avoiding the term HGBCL in pediatric population, and DH is absent in this age range, there are tumors that show intermediate features between the two entities resembling the high-grade morphology observed in adults, as well as a subset of DLBCL with *MYC*-R. In children, adolescents, and young adults (CAYA), both BL and DLBCL have well-defined mutational profiles [16–18]. In CAYA DLBCL, this profile differs from the observed in the adult population [17], whereas in BL, the mutational profile is shared between age groups but with different incidences of the mutated genes according to age [19, 20]. Although since the 4th WHO classification [21] a wider morphological spectrum is avowed in BL, this assumption is based in gene expression profiling (GEP) as the very well-known molecular BL (mBL) signature described by the German Consortium [22–24], but no mutational studies have been performed to demonstrate that BL with atypical morphology share the mutational profile of prototypic BL. In comparison to adult disease, the overall prognosis of pediatric B-cell non-Hodgkin lymphoma (B-NHL) is excellent, although relapses still confer poor outcomes [25]. Nowadays, risk stratification of these patients relies on clinical biomarkers such as elevated lactate dehydrogenase levels and advanced stage (III–IV) [26]. However, there is a clear need for predictive biological biomarkers for survival at progression or relapse. Recent genomic studies have determined the association of *TP53* alterations with a worse outcome [17, 19]. Nevertheless, whether the morphological features of these tumors and the inclusion of HGBCL, NOS as a diagnostic category could be a prognostic indicator remains unclear in this age group.

Overall, considering the rarity of these aggressive tumors with overlapping features between BL and DLBCL in CAYA and the challenges in differentiating them by conventional molecular approaches, we performed an integrated genomic analysis aiming to refine the understanding of the pathobiology of these lymphomas, the borders among these two entities, and improve diagnostic accuracy.

METHODS

Patients and samples

We searched for aggressive B-cell lymphomas diagnosed in CAYA patients up to 35 years old. Biopsies and clinical data from 32 pediatric patients (up to 18 y) were recruited from Spanish centers belonging to Sociedad Española de Hematología y Oncología Pediátricas (SEHOP), and five young adult cases (18–33 y) were retrieved from the files of Hospital Clínic of Barcelona (Table 1, Supplementary Table S1).

Cases were selected from the national centralized pathology review of the tumors of the Spanish national registry of pediatric and adolescent lymphomas. The original diagnoses of the submitted cases were 13 BL, 8 HGBCL, NOS, 6 B-cell lymphomas suggestive of BL, 5 HGBCL-BCLU, and 5 DLBCL. DH-lymphomas, lymphomas bearing the characteristic 11q gain/loss aberration of large/high-grade B-cell lymphoma with 11q-aberration (LBCL/HG-11q), and prototypical BL were excluded [2, 3]. All samples were collected at diagnosis except for case HG8, analyzed at progression. Eleven cases were previously published [17]. The morphology details such as the presence of starry sky pattern, cell pleomorphism, nuclei size and irregularity, Burkitt-like chromatin, and necrosis were evaluated on H&E stain of each case (Supplementary Table S2).

The tumors were reclassified by the pathology panel (NCdA, LW, EC, and OB), blinded to the original diagnosis and *MYC*-R status [1], as 29 high-grade B-cell lymphomas with intermediate features between BL and DLBCL, 4 HGBCL with blastoid morphology and 4 DLBCL (Supplementary Table S1). All samples investigated contained more than 60% of neoplastic cells. This study was approved by the Hospital Clínic of Barcelona Ethics Review Board (HCB/2021/0847) and in accordance with the Declaration of Helsinki. Informed consent was obtained from all patients.

Immunohistochemistry and fluorescence in situ hybridization (FISH)

The immunophenotype was studied using standard immunohistochemistry (IHC) protocols on an automated platform (Ventana BenchmarkUltra, Roche, Basel, Switzerland). EBV status was determined by in situ hybridization (Epstein–Barr virus-encoded small RNA, EBER) (Supplementary Table S3). FISH analyses were performed using standard protocols. Breaks at *BCL2, BCL6, MYC,* and IGH, t(8;14) translocation and 11q alterations were analyzed using commercial FISH probes (Metasystems, Altlußheim, Germany; Agilent Technologies, Santa Clara, CA; Abbot, Chicago, IL; ZytoVision, Bremerhaven, Germany).

Targeted NGS for structural variants (SV) and mutational analysis

For the study of SV and mutations, a custom capture panel (SureSelectXT, Agilent Technologies, Santa Clara, CA) was used for the analysis of 26 tumor samples (Supplementary Methods, Table S4, and Fig. S1). Libraries were indexed and compatible with the NextSeq 2000 (Illumina, San Diego, CA) instrument. SV and mutations were called following the respective in-house pipelines (Supplementary Methods and Supplementary Fig. S2). Mutational information from five additional previously published cases was retrieved [17]. Sanger sequencing for *TP53* mutational analysis [27] and *MYC* breakpoint verification were performed in isolated cases.

DNA copy number (CN) alterations analysis

CN alterations were examined using OncoScan ($n = 30$) or CytoScan platforms ($n = 5$) (Thermo Fisher Scientific, Waltham, MA, USA) (Supplementary Methods) and evaluated using Nexus Copy Number v9.0 (Bionano, San Diego, CA, USA). Previously published CN data were used for comparison [17, 28].

Gene expression profile

Digital GEP was performed using the DLBCL90 assay [10] and/or Lymphoma Subtyping Test-Lymph2Cx (NanoString Technologies, Seattle, WA) to assign DZsig and COO status, respectively (Supplementary Methods).

Statistical methods

Fisher's exact test was utilized for discrete variables, while the Wilcoxon rank sum exact test and Student t-test were employed for continuous variables. The Kaplan–Meier method was used to estimate event-free survival (EFS). Hazard risk was assessed using the Cox proportional hazards model and comparisons were performed using the Log Rank test. Statistical significance was set at 0.05 and *p*-values were two-sided. Analyses were carried out with R v4.1.1.

RESULTS

Clinicopathological characteristics

The 37 patients included in the study were 32 children and adolescents and 5 young adults. Twenty-seven (73%) were male, and 10 (27%) were female, with a median age at diagnosis of 12 years (range 3-33) (Table 1, Supplementary Table S1). Twelve (32%) patients presented with nodal disease, whereas 25 (68%) had extranodal presentation, the gastrointestinal tract (60%) being the most frequently affected site. Among patients with available clinical information, 25 (69%) had advanced-stage disease (III–IV). Thirty-three patients (89%) were treated using pediatric B-NHL high-intensity protocols, 3 (8%) received R-CHOP and 1 patient (3%) Burkimab dose-intense immunochemotherapy. Fourteen patients (38%) were treated with rituximab in combination with chemotherapy and two cases underwent autologous hematopoietic stem cell transplantation as consolidation in first-line treatment. Upon pathological review, most tumors (33/37) had a high-grade morphology, 29 with features intermediate between DLBCL and BL, and 4 with blastoid cytology. Four cases showed DLBCL morphology and were included in the study due to the presence of *MYC*-R that likely lead to the original diagnosis of BL (Fig. 1, Supplementary Tables S1 and S2). Some cases, initially diagnosed as BL, were included in the study as HGBCL due to the atypical morphology with marked irregular nuclei, pleomorphism or blastoid features, intense BCL2 expression, and/or negative detection of *MYC* rearrangement by routine techniques

Table 1. Clinical features of 37 aggressive B-cell NHL with overlapping features between DLBCL and BL according to *MYC*-R status.

	***n* = 37**	***MYC*-non-R *n* = 15 (41%)**	***MYC*-R *n* = 22 (59%)**	***P*-value[a]**
Sex				0.7
Female	10 (27%)	5 (33%)	5 (23%)	
Male	27 (73%)	10 (67%)	17 (77%)	
Mean age at diagnosis (range)	13 (3–33)	15 (8–33)	11 (3–29)	0.017
Age Group				0.4
Children	32 (86%)	12 (80%)	20 (91%)	
Young Adults	5 (14%)	3 (20%)	2 (9%)	
Mean months of follow-up (range)	46 (1–277)	66 (1–277)	33 (1–123)	0.5
Stage[b]				0.14
I–II	11 (30%)	7 (47%)	4 (18%)	
III–IV	25 (67%)	9 (53%)	17 (77%)	
Unknown	1 (3%)	-	1 (5%)	
Extranodal involvement				0.7
Yes	25 (68%)	11 (73%)	14 (64%)	
No	12 (32%)	4 (27%)	8 (36%)	
Gastrointestinal location				0.5
Yes	15 (41%)	7 (47%)	8 (36%)	
No	22 (59%)	8 (53%)	14 (64%)	
Treatment strategy				0.9
BFM-Based	2 (5%)	1 (7%)	1 (5%)	
Burkimab	1 (3%)	-	1 (5%)	
CHOP	3 (8%)	2 (13%)	1 (5%)	
LMB-Based	31 (84%)	12 (80%)	19 (85%)	
Rituximab at first-line therapy				0.6
Yes	14 (38%)	5 (33%)	9 (41%)	
No	23 (62%)	10 (67%)	13 (59%)	
LDH levels				0.14
High	12 (40%)	3 (20%)	9 (41%)	
Normal	18 (60%)	11 (67%)	8 (36%)	
Unknown	7	2 (13%)	5 (23%)	
Hematopoietic stem cell transplantation				>0.9
Yes	2 (5%)	1 (7%)	1 (5%)	
No	31 (84%)	13 (86%)	18 (82%)	
Unknown	4 (11%)	1 (7%)	3 (13%)	
Relapse				>0.9
Yes	5 (14%)	2 (13%)	3 (14%)	
No	32 (86%)	14 (87%)	18 (86%)	
Status				0.063
Deceased[c]	6 (16%)	-	6 (29%)	
Alive	31 (84%)	16 (100%)	15 (71%)	

[a]Fisher's exact test.
[b]Stage was established according to the St. Jude/International Pediatric NHL Staging System or Ann Arbor staging system for pediatric and adult patients, respectively.
[c]Two patients deceased due to complications related to lymphoma disease.

(Supplementary Tables S1 and S2). All cases except one had a germinal center (GC) phenotype according to the Hans algorithm [29]. In line with these results, the Lymph2Cx assay identified only 3/33 (9%) activated B-cell-like (ABC) tumors and 1/33 (3%) unclassified. Of the 28 cases in which TdT expression was investigated, only one showed scattered positivity. MUM1/IRF4 was negative in 23/34 studied cases. Eleven out of 36 investigated cases expressed BCL2, whereas LMO2, a GC marker downregulated in BL and other *MYC*-R lymphomas [30], was negative in 11/25 (44%) analyzed cases. In detail, only three of the 14 LMO2-positive cases harbored *MYC*-R, while 9/11 LMO2-negative cases had *MYC-R*; notably one of the LMO2-negative *MYC*-non-R cases was a CD10-negative ABC tumor (HG4) [31]. Using a 40% cut-off [32], 15/30 (50%) cases were positive for MYC expression by IHC. Additionally, three of 35 evaluated cases

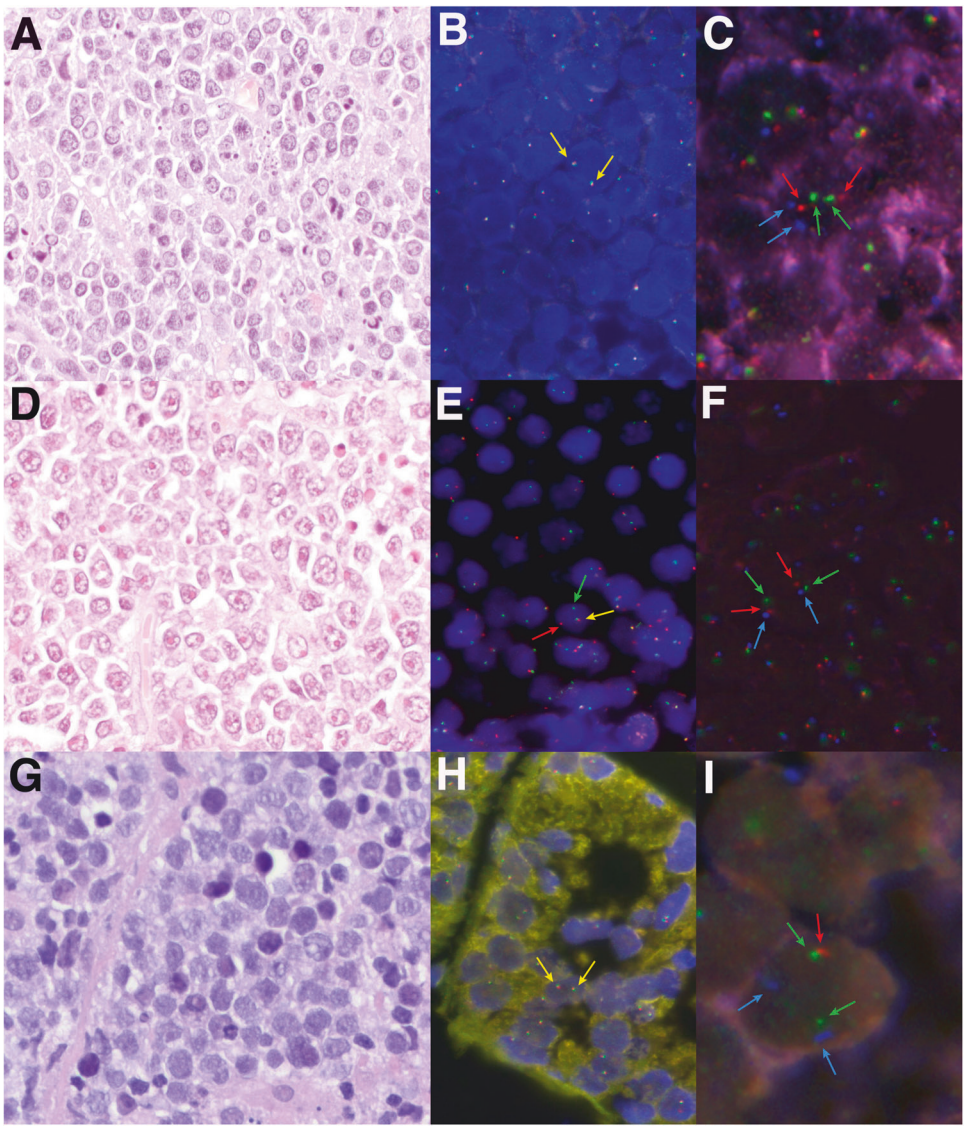

Fig. 1 Morphological, immunohistochemical, and genetic features of three high-grade cases. A Case HG28 showed a diffuse proliferation of medium-sized lymphocytes with slight pleomorphism, irregular nuclei, and apoptotic bodies consistent with features intermediate between BL and DLBCL (H&E, original magnification at 400×). **B** *MYC* break-apart FISH probe showed two colocalizations in each cell consistent with the absence of gene rearrangement. **C** FISH analysis for 11q-aberration showed 2 green (11q23.3 minimal region gain, MRG), 2 orange (11q24.3 minimal region loss, MRL), and 2 aqua (CEN11 D11Z1) signals, compatible with a non-altered 11q chromosomal region. **D** Case HG33 depicted a DLBCL morphology showing a predominance of large centroblastic lymphocytes (H&E, original magnification at 400×). **E** *MYC* break-apart FISH probe showed one red signal, one green signal, and one colocalization, consistent with the rearrangement of the gene. **F** FISH analysis for 11q-aberration showed 2 green (11q23.3 MRG), 2 orange (11q24.3 MRL), and 2 aqua (CEN11 D11Z1) signals constellation, compatible with a non-altered 11q chromosomal region. **G** Case HG39 consisted of monotonous medium-sized lymphocytes with blastoid appearance (H&E, original magnification at 400×). **H** *MYC* break-apart FISH probe showed two colocalizations consistent with a non-rearranged pattern. **I** A non-prototypic terminal deletion of 11q24.3 region was identified in case HG39. The FISH constellation showed 2 green (11q23.3 MRG), 1 orange (22q24.3 MRL), and 2 aqua (CEN11 D11Z1) signals.

were EBER-positive and SOX11 was expressed in 3/28 (11%) cases. Interestingly, MYC, EBER, and SOX11 positivity was restricted to *MYC*-R cases, and the mutual exclusivity of SOX11 expression and EBV-positivity reported in BL [33] was confirmed (Supplementary Fig. S3).

MYC translocations were detected by FISH break-apart (BAP) and/or dual-fusion (DF) probes in 19 out of 37 tumors, including the 4 DLBCL. Three of the 19 *MYC*-R cases were only detected using the DF probe (Supplementary Fig. S3). Two *MYC*-non-R tumors carried *BCL6* breaks. No *BCL2*-R were detected. However, 6 *MYC*-R cases expressed BCL2 by IHC, although only two with a diffuse and intense pattern. Fifteen out of the 19 *MYC*-R cases studied expressed MYC by IHC. Accordingly, MYC RNA levels were significantly higher in *MYC*-R than in *MYC*-non-R cases ($P < 0.001$) (Supplementary Fig. S4). Although tumors with prototypical 11q-aberrations were excluded in the study, we found 3 cases that displayed 11q24.3 terminal deletions only (HG39, HG40, and HG53), and one of them (HG53) also carried a *MYC* break.

Identification of SV by targeted NGS

Twenty-six tumors were analyzed by our SV-NGS approach. The mean targeted coverage was 238× (range: 95–747). A total of 13 high-quality SV (11 targeting *MYC* and 2 *BCL6*) were identified (Supplementary Table S5). *MYC* and *BCL6* rearrangements detected by FISH were verified in 11 out of 12 tumors (92%) by the SV-NGS panel. This strategy also identified two additional t(8;14)-positive cases (HG11 and HG29) not recognized by FISH. No other recurrent rearrangements nor DH cases were observed (Fig. 2A). In cases HG4

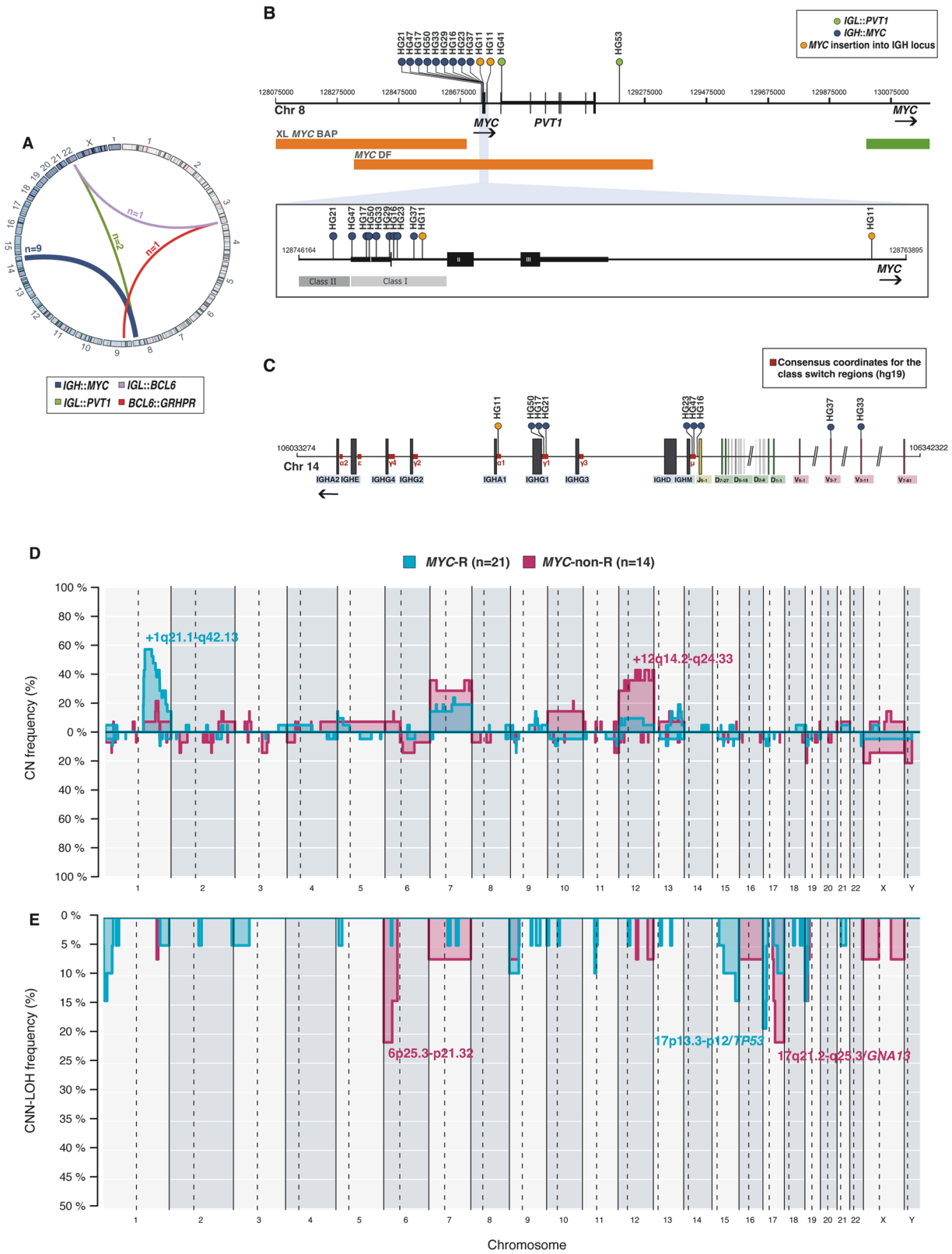

Fig. 2 SV architecture of 35 aggressive B-cell lymphomas with overlapping features between BL and DLBCL. A SV discovered by targeted NGS sequencing ($n = 26$). **B** Location of the breakpoints identified in the *MYC* gene. **C** Location of breakpoints in the IGH locus according to current consensus coordinates [37]. **D**, **E** Comparative plot of CN and CNN-LOH alterations among the 2 genetic groups based on *MYC* rearrangement status. Light blue identifies *MYC*-R cases ($n = 21$), whereas dark pink identifies *MYC*-non-R tumors ($n = 14$).

and HG34, *BCL6* partners were IGL (22q11) and *GRHPR* (9p13), respectively. The *GRHPR* gene has been previously described as *BCL6* partner in follicular lymphoma [34] and DLBCL [35]. In our series, 73% (8/11) of the reported *MYC* breakpoints were in the first exon or intron of the gene, thereby classified as class I [36]. Conversely, only one case (HG21) demonstrated a class II breakpoint located immediately upstream of *MYC*. Although no class III breakpoints far upstream *MYC* were identified, cases HG41 and HG53 exhibited *IGL::PVT1* translocations with breakpoints downstream of *MYC* (Fig. 2B). Meanwhile, HG11 harbored a four-breakpoint complex *IGH::MYC* rearrangement that juxtaposed the *MYC* coding exons 2 and 3 and the class-switch region (CSR) of IGHA1 (Fig. 2C, Supplementary Fig. S5) [14, 37]. IG breakpoints probably resulted from aberrant CSR in 5 cases and from aberrant somatic hypermutation (SHM) in 4 cases (Supplementary Table S5).

Copy number alteration profile

CN analysis detected genetic alterations in 31/35 investigated tumors (mean 6.8 alterations/case; range 0–27 alterations) and a total of 55 regions of CNN-LOH in 29 cases (Supplementary Table S6). No significant differences in the genetic complexity according to age were identified ($P = 0.23$) (Supplementary Fig. S6A). This level of complexity was similar to that observed in BL and CAYA DLBCL (Supplementary Fig. S6B) [17, 28]. Recurrent CN alterations (observed in >15% of tumors) included gains in 1q21.1-q42.13, 13q31.3/*MIR17HG*, chr7, and 12p13.31-q24.33. Frequent CNN-LOH (>10%) involved 6p22.1-p21.32, 17p13.3-p12/*TP53*, 17q21.32-q24.3/*GNA13*, and 19p13.3-13.2/*CD70* regions. Homozygous deletions at 9p21.3/*CDKN2A* and 19p13.3-p13.2/*CD70* were observed in three cases each. Chromothripsis-like patterns were detected in 4 cases that showed shattered pattern on chromosomes 1, 2, 12, and 13 (Supplementary Fig. S7A). Moreover, in case HG8 we identified a CN profile indicative of a cryptic *MYC* rearrangement with a gain and loss pattern at 8q24.21, suggesting the existence of a break at 3′ of the gene (Supplementary Fig. S7B, C).

Although tumors with the prototypical 11q-aberration were excluded, we confirmed by CN the presence of 11q24.3 deletions in three cases previously observed by FISH. In case HG53, the alteration was a focal 126 kb 11q24.2-q24.3 deletion not including the whole telomeric region seen in LBCL/HG-11q (Supplementary Fig. S8).

We also investigated the CN profile based on the *MYC*-R status. *MYC*-R cases exhibited frequent 1q21.2-q32.1 gains (57%), whereas gains at 12q14.2-q24.33 were recurrent in *MYC*-non-R tumors (43%). Furthermore, *MYC*-R tumors recurrently showed CNN-LOH at 17p13.3-p12/*TP53* (19%), while 6p25.3-p21.32 (21%) and 17q21.2-q25.3/*GNA13* (21%) CNN-LOH were characteristic of *MYC*-non-R tumors (Fig. 2D, E). Gains/amplifications of *MIR17HG* loci have been suggested to be alternative mechanisms of *MYC* dysregulation [13]. In our series, 3/5 tumors with *MIR17HG* gains/amplifications harbored *MYC* rearrangements. A tendency towards a higher complexity was observed in *MYC*-non-R cases (8.1 vs 5.9 alterations/case, $P = 0.076$). The CN profile of our *MYC*-R tumors was similar to that reported in BL [28] with both groups of tumors sharing gains of 1q21.1-q44 and chr7, and 17p deletions (Supplementary Fig. S6C).

Mutational analysis by targeted NGS

A total of 258 potential driver mutations were identified in the 31 analyzed tumors (mean 8.3 mutations/case) (Fig. 3, Supplementary Table S7 and Supplementary Methods). No significant differences in terms of mutational burden were observed between adult and pediatric cases (7.6 vs 8.5 mutations/case, $P = 0.62$). Globally, the most frequently mutated genes were *MYC* (39%), *ID3* (35%), *P2RY8* (35%), *DDX3X* (32%), *GNA13* (29%), and *FOXO1* and *TP53* (26%). In case HG46, a *TP53* mutation was identified by Sanger sequencing.

A trend towards a higher number of mutations was observed in *MYC*-R tumors, including the 4 DLBCL, compared to *MYC*-non-R tumors (9.3 and 7.1 mutations/case, $P = 0.085$) and their mutational profiles were clearly different. In detail, driver mutations in *MYC*, *ID3,* and *TP53* were significantly more recurrent in *MYC*-R tumors (71%, 59%, and 50%, respectively) than in those without *MYC* translocations (0%, 7%, and 0%) (*P-adjusted* < 0.05). *MYC* variants mostly clustered around N-terminal phosphorylation sites (Fig. 3B) and all the *ID3* mutations affected the helix-loop-helix domain, potentially impairing ID3 function. *TP53* mutations were generally localized in exons 5 to 8 and affected the *TP53* DNA-binding domain (Fig. 3B). Furthermore, in 4/9 mutated cases, *TP53* mutations were accompanied by 17p CNN-LOH or loss. *DDX3X* mutations were also predominant in *MYC*-R tumors (47% vs 14%) and were mainly localized on the helicase domain. Nine out of the ten patients with *DDX3X* mutations were male. *MYC*-R tumors also had recurrent alterations in *FOXO1* (41%) and *CCND3* (35%), and mutations in the component of the SWI-SNF chromatin remodeling complex *ARID1A* (35%). Overall, the genetic landscape observed in *MYC*-R tumors resembled the one depicted in sporadic BL (sBL) [38], although we did not find any *TCF3* mutation and we observed a tendency towards a higher frequency of *P2RY8* alterations in our series (31% vs 9%, *P-adjusted* = 0.16) (Supplementary Fig. S9).

Conversely, the mutational profile of *MYC*-non-R tumors clearly differed from the BL-like profile observed in *MYC*-R tumors, having a more heterogeneous mutational landscape closer to that reported in DLBCL. In detail, the most recurrent alterations involved *GNA13* (50%), *P2RY8* (38%), *CARD11* and *NFKBIE* (29%), and *EBF1* (23%) genes. Additionally, *EZH2* mutations were found in two cases. Sixty-four percent of *MYC*-non-R tumors had mutations affecting either *GNA13* or *P2RY8*, but the previously reported mutual exclusivity of *GNA13* and *P2RY8* mutations on DLBCL [39] could not be confirmed. *CARD11* was solely found mutated in *MYC*-non-R tumors and 83% of the mutations occurred in the coiled-coil domain (Fig. 3B), known to produce NF-κB pathway constitutive activation [40]. Furthermore, 29% of *MYC*-non-R tumors displayed mutations in *NFKBIE*, an inhibitor of the NF-κB pathway. Interestingly, among these, 3/4 mutated cases carried the previously described frameshift 4-bp deletion p.Y254fs (Fig. 3B) [41]. Isolated mutations in other B-cell receptor signaling pathway genes including *IKBKB*, *BCL10*, *NFKBIA,* and *MAP2K1* were also observed among the *MYC*-non-R. Overall, 71% of the *MYC*-non-R cases had mutations targeting the B-cell receptor signaling pathway as confirmed by a pathway enrichment analysis (Supplementary Table S8). However, *MYC*-non-R cases lacked other characteristic mutations of adult GCB (*KMT2D*) and ABC-DLBCL (*MYD88*^{L265P} and *CD79B*) [42], as well as *SOCS1* mutations specifically seen in CAYA DLBCL (Supplementary Fig. S10) [17]. Furthermore, when we attempted to classify these tumors in the molecular genetic subtypes described in adult DLBCL [43–45], only one of the 31 investigated cases was classified (HG4, BN2 subgroup).

Dark zone signature prediction

Expression of the DZsig was observed in 15 of the 27 (56%) investigated tumors (Fig. 3C), with 14 (93%) having GCB COO and one with unclassifiable COO (HG44). Thirteen out of the sixteen (81%) *MYC*-R tumors were DZsig^{pos}, 1/16 was DZsig^{ind} and GCB COO, and 2/16 had ABC COO (Fig. 3C; Supplementary Fig. S11). No DZsig^{neg} cases were identified among those tumors with *MYC* rearrangements. In contrast, most *MYC*-non-R tumors were DZsig^{neg} (6/11, 55%) or DZsig^{ind} (2/11, 18%). One case had an ABC profile, and only two (18%) *MYC*-non-R cases expressed the DZsig, one of them with high MYC RNA expression levels (NM_002467.3 from DLBCL90 assay [10]) close to those observed in *MYC*-R lymphomas (Fig. 3D). Interestingly, 92% of GCB *MYC*-R cases expressed the DZsig, whereas DZsig expression was only observed in 20% of GCB *MYC*-non-R tumors ($P < 0.001$).

Prognostic value of clinical and molecular features

The 3-year EFS of the whole series was 79.6% (95% CI 67.2–94.4%), increasing to 83.4% (95% CI 69.6–92.4%) when focusing only on

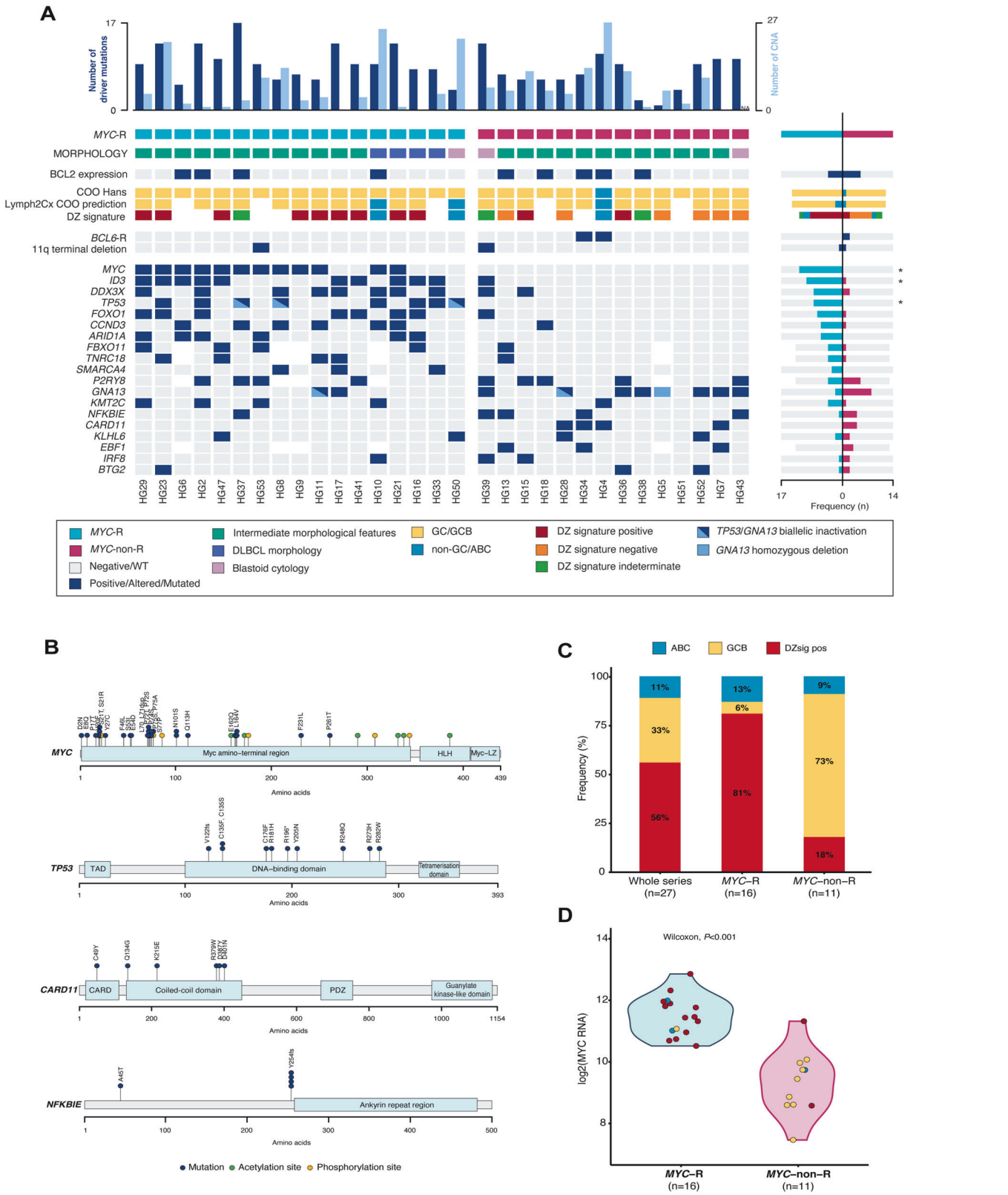

the pediatric population (<19 y). Although we assessed the impact of several clinical and molecular features in the outcome of our patients (Supplementary Table S9), only *TP53* and *KMT2C* mutations defined poor-prognosis groups (3-year EFS, *TP53*: 91% vs 39% $P < 0.05$; *KMT2C*: 83% vs 40% $P < 0.05$) (Supplementary Table S9 and Fig. S12).

DISCUSSION

HGBCL, NOS is a morphological category originally conceived to accommodate borderline aggressive B-cell lymphomas that cannot be reliably classified as BL, DLBCL, or HGBCL-DH, based on the defined morphological, immunophenotypic, and molecular criteria. The particularities of these cases still raise some

Fig. 3 Molecular CN and mutational information on 31 B-cell lymphomas with overlapping features between BL and DLBCL. A Oncoprint showing gene expression, mutations, and CN characteristics by case. Each column corresponds to a case, the light blue bars in the top histogram depict the number of CNA while the dark blue bars represent the number of driver mutations. Each row of the bottom plot represents a gene. Only genes with driver mutations in more than 2 cases are represented. Asterisks identify significant differences according to adjusted (FDR) Fisher's exact test (*P-adjusted* < 0.05). **B** Diagram of the relative positions of driver mutations is shown for *MYC*, *TP53, CARD11,* and *NFKBIE* genes, x-axes indicate amino acid position. MYC domains (HLH, helix-loop-helix; MYC-LZ, leucine zipper; TAD, transactivation domain). TP53 domains (DBD: DNA-binding domain); TAD: transcription activation domain; CARD11 (CARMA1) domains (CARD, caspase activation, and recruitment domain; PDZ, PDZ containing domain). **C** Proportion of DZsig positive tumors in the whole analyzed series ($n = 27$) and according to *MYC*-R status. **D** MYC RNA expression (NM_002467.3) according to DZsig and COO categorization and *MYC*-R status.

uncertainty, and the diagnosis of HGBCL, NOS in the pediatric population was not recommended in the revised 4th WHO classification [1]. Nevertheless, pathologists observe tumors with overlapping features between DLBCL and BL in CAYA, emphasizing the need for a better understanding of the biological insights and clinical significance of these lymphomas.

To fill this knowledge gap, we searched our files for cases of HGBCL with BCLU, HGBCL-blastoid or DLBCL with *MYC* rearrangement in patients up to 35 years old. Most accrued cases showed an intermediate morphology between BL and DLBCL, featuring medium-sized nuclei with irregular contours and pleomorphism, nine of them with BCL2 expression (Supplementary Table S1 and S2). As expected in this age range, 97% of the cases were GCB, including the three EBV-positive tumors. Integrated FISH and NGS approach confirmed *MYC* rearrangements as the most prevalent SV within our series, affecting 59% of the whole series and 55% of those tumors with high-grade morphology. *MYC* rearrangement status distinguished two genetically differentiated subgroups.

In contrast to adult patients in the context of these morphological features, *BCL2*-R and DH-lymphomas were absent, as previously seen in pediatric B-NHL, and we only observed *BCL6* rearrangements in two *MYC*-non-R cases [46]. BCL2 expression has been described in a subset of BL, mainly in adult patients [47]. In our series, 31% of cases expressed BCL2, without association with age or presence of *MYC* rearrangement. Only in one *MYC*-R case, BCL2 overexpression could be explained by the presence of 18q12.3-q23/*BCL2* gain. LMO2 is a GC marker downregulated in *MYC*-R lymphomas. In line with the previous series [31], our cases showed a significant inverse correlation between LMO2 expression and the presence of the *MYC*-R in GCB, CD10 positive tumors ($P < 0.001$). In our series, 3/16 (19%) *MYC*-R tumors expressed SOX11, a frequency relatively lower than that recently described in pediatric and adult BL (43–56%) [33, 48].

Regarding the architecture of *MYC* rearrangements, *MYC* breakpoints in this cohort mainly clustered in the first exon/intron of *MYC* (class I), in line with pediatric sBL [49]. This *MYC* breakpoint distribution contrasts with the one observed in adult single-hit *MYC*-R DLBCL and HGBCL-DH, in which class I/II breaks accounted only for 41% and 28% of *MYC* breaks, respectively [12, 50]. In contrast to DH in adults where the partner genes in *MYC* translocations are more promiscuous [12, 50], in our study, IG loci were the only *MYC* partners identified, and as reported for pediatric sBL [49], abnormal CSR and SHM were the predominant mechanisms leading to *IG::MYC* translocations. Altogether, these findings indicate that, regardless of their high-grade or DLBCL morphology, *MYC* translocations in these *MYC*-R tumors arise in a similar way to those in sBL. The SV-NGS strategy also demonstrated the absence of cryptic rearrangements targeting *MYC* or *BCL2* with the exception of the cryptic *IGH::MYC* rearrangement observed in case HG11. It also identified the t(8;14) translocation in one case (HG29) not previously recognized by FISH, probably due to technical issues (see Supplementary Discussion).

MYC-R tumors, including the DLBCL, also shared mutational and CN profiles with BL. The CN profile of our *MYC*-R tumors virtually overlapped with the observed in BL, with recurrent 1q21.1-q44 gains and 17p CNN-LOH and deletions [28]. All *MYC*-R cases studied harbored exonic and/or multiple intronic *MYC* mutations. Somatic mutations in *ID3*, *DDX3X*, *TP53*, *FOXO1*, *CCND3,* and *ARID1A*, previously described to cooperate with *MYC* dysregulation in BL development, were also recurrently found in *MYC*-R tumors [51]. In this sense, most of our *MYC*-R cases presented genetic features characteristic of the prevalent molecular subgroups recently defined in BL [20], IC-BL (mutations in *ID3* and *CCND3*), and DGG-BL (mutations in *DDX3X*, *GNA13,* and *GNAI2*). Importantly, this mutational landscape resembling the one reported in BL was not observed in any *MYC*-non-R tumors, except for HG39. Moreover, virtually all *MYC*-R tumors with GCB COO expressed the DZsig as previously reported for BL [11]. Of note, the features observed in our CAYA *MYC*-R DLBCL contrast with a previous study where those tumors did not align with the GEP of mBL [52]. Conversely, the mBL signature captured other *MYC*-non-R mature B-cell lymphomas in CAYA that in later studies turned out to be identified as LBCL/HG-11q [53].

The mutational landscape of *MYC*-non-R cases was closer to that observed in DLBCL (*GNA13*, *CARD11*, *NFKBIE, EZH2*) but did not fully mimic adult or CAYA DLBCL [7, 17]. In detail, *KMT2D* mutations, previously reported in 39% of adult GCB-DLBCL [42], 23% of CAYA DLBCL, NOS [17], and also observed in 43% of adult HGBCL, NOS [4, 7], were absent among *MYC*-non-R tumors (Supplementary Fig. S10). Similarly, these tumors also lacked mutations of ABC-DLBCL such as $MYD88^{L265P}$ or *CD79B*. Moreover, only one of our *MYC*-non-R cases showed a *SOCS1* mutation, while this gene has been found mutated in up to 27% of CAYA DLBCL [17].

Of note, only one of our *MYC*-non-R tumors was classified as BN2 by the *LymphGen* algorithm [45], suggesting that despite their similarities, they do not fit in the established adult DLBCL genetic subgroups. Further studies are needed to elucidate whether these *MYC*-non-R tumors with high-grade morphology constitute a genetically differentiated entity.

Concomitant *MYC* translocations and 11q-aberrations have been previously described, suggesting that the spectrum of malignancies with 11q-aberration was broader than previously assumed [54, 55, 56]. Although the presence of the prototypical 11q-aberration [3] was an exclusion criterion for entering the series, two of the cases analyzed by NGS showed only terminal 11q deletions by FISH and CN array; one was negative for *MYC*-R (HG39) and the other carried a t(8;22) translocation (HG53) [55, 57]. Interestingly, both cases displayed mutational profiles closer to BL than the ones previously reported in LBCL/HG-11q [14, 57]. These results confirm that the detection of an 11q telomeric loss only is not sufficient to classify the cases as LBCL/HG-11q and that an integrative morphological and broader molecular approach is necessary. Nevertheless, further studies in larger series of tumors are needed to ratify this observation.

Clinically, differently to what is described in adult HGBCL [4], this specific morphological constellation does not seem to clearly select a group of patients with poor outcomes, although our pediatric cases had an inferior outcome compared to other recently published pediatric B-NHL cohorts (83% vs 94%) [26]. Nevertheless, it is worth mentioning that our cohort is not only

small in number but also highly selected and heterogeneously treated (only 67% of pediatric high-risk patients treated with rituximab) therefore, comparisons cannot be properly performed. Future prospective trials should clarify this issue. No differences were observed in terms of survival between patients with *MYC*-R and *MYC*-non-R tumors. However, *TP53* mutations, that were exclusively seen in *MYC*-R lymphomas in our cohort, defined a poor-prognosis group, as previously reported in pediatric aggressive B-cell lymphomas [19, 27].

To the best of our knowledge, we provided herein an integrative molecular and clinical characterization of aggressive CAYA B-NHL in the morphological spectrum between BL and DLBCL. Our results demonstrated that the genetic profile of these tumors is heterogeneous, but for the first time, we have clearly distinguished two genetically defined subgroups based on *MYC*-R status regardless of the morphology. One group carrying *MYC*-R that should be diagnosed as BL, whereas the second group had a mutational profile closer to DLBCL that needs to be further investigated. Although FISH routine techniques used in clinical diagnostics capture most *MYC* translocations, our findings confirmed that some tumors may harbor cryptic rearrangements that FISH can miss. DZsig expression and a BL-related mutational profile, would support a BL diagnosis in these cases and suggest the presence of a cryptic *MYC* rearrangement that could be confirmed by an SV-NGS approach. In Supplementary Fig. S13, we suggest how all the information derived from our study would expand BL diagnostic criteria and could be applied in the diagnostic workup of aggressive CAYA B-NHL in the morphological spectrum between BL and DLBCL.

DATA AVAILABILITY

Copy-number data reported in this article have been deposited at GEO database under accession number GSE252974. Sequencing data have been deposited to the European Nucleotide Archive (ENA) under the accession number PRJEB71882.

REFERENCES

1. Swerdlow SH, Campo E, Harris NL, Jaffe ES, Pileri SA, Stein H, et al., editors. WHO classification of tumours of haematopoietic and lymphoid tissues. Revised 4th ed. Lyon: IARC; 2017.
2. Alaggio R, Amador C, Anagnostopoulos I, Attygalle AD, Araujo IBO, Berti E, et al. The 5th edition of the World Health Organization classification of haematolymphoid tumours: lymphoid neoplasms. Leukemia. 2022;36:1720–48.
3. Campo E, Jaffe ES, Cook JR, Quintanilla-Martinez L, Swerdlow SH, Anderson KC, et al. The international consensus classification of mature lymphoid neoplasms: a report from the Clinical Advisory Committee. Blood. 2022;140:1229–53.
4. Olszewski AJ, Kurt H, Evens AM. Defining and treating high-grade B-cell lymphoma, NOS. Blood. 2022;140:943–54.
5. Ok CY, Medeiros LJ. High-grade B-cell lymphoma: a term re-purposed in the revised WHO classification. Pathology. 2020;52:68–77.
6. Perry AM, Crockett D, Dave BJ, Althof P, Winkler L, Smith LM, et al. B-cell lymphoma, unclassifiable, with features intermediate between diffuse large B-cell lymphoma and Burkitt lymphoma: study of 39 cases. Br J Haematol. 2013;162:40–9.
7. Collinge BJ, Hilton LK, Wong J, Ben-Neriah S, Rushton CK, Slack GW, et al. Characterization of the genetic landscape of high-grade B-cell lymphoma, NOS - an LLMPP project. Hematol Oncol. 2021;39:781–4.
8. Momose S, Weißbach S, Pischimarov J, Nedeva T, Bach E, Rudelius M, et al. The diagnostic gray zone between Burkitt lymphoma and diffuse large B-cell lymphoma is also a gray zone of the mutational spectrum. Leukemia. 2015;29:1789–91.
9. Sha C, Barrans S, Cucco F, Bentley MA, Care MA, Cummin T, et al. Molecular high-grade B-cell lymphoma: Defining a poor-risk group that requires different approaches to therapy. J Clin Oncol. 2019;37:202–12.
10. Ennishi D, Jiang A, Boyle M, Collinge B, Grande BM, Ben-Neriah S, et al. Double-hit gene expression signature defines a distinct subgroup of germinal center B-cell-like diffuse large B-cell lymphoma. J Clin Oncol. 2019;37:190–201.
11. Alduaij W, Collinge B, Ben-Neriah S, Jiang A, Hilton LK, Boyle M, et al. Molecular determinants of clinical outcomes in a real-world diffuse large B-cell lymphoma population. Blood. 2023;141:2493–507.
12. Chong LC, Ben-Neriah S, Slack GW, Freeman C, Ennishi D, Mottok A, et al. High-resolution architecture and partner genes of MYC rearrangements in lymphoma with DLBCL morphology. Blood Adv. 2018;2:2755–65.
13. Hilton LK, Tang J, Ben-Neriah S, Alcaide M, Jiang A, Grande BM, et al. The double-hit signature identifies double-hit diffuse large B-cell lymphoma with genetic events cryptic to FISH. Blood. 2019;134:1528–32.
14. Wagener R, Bens S, Toprak UH, Seufert J, López C, Scholz I, et al. Cryptic insertion of MYC exons 2 and 3 into the immunoglobulin heavy chain locus detected by whole genome sequencing in a case of "MYC-negative" Burkitt lymphoma. Haematologica. 2020;105:e202–5.
15. King RL, McPhail ED, Meyer RG, Vasmatzis G, Pearce K, Smadbeck JB, et al. False-negative rates for MYC fluorescence in situ hybridization probes in B-cell neoplasms. Haematologica. 2019;104:e248–51.
16. Love C, Sun Z, Jima D, Li G, Zhang J, Miles R, et al. The genetic landscape of mutations in Burkitt lymphoma. Nat Genet. 2012;44:1321–5.
17. Ramis-Zaldivar JE, Gonzalez-Farré B, Balagué O, Celis V, Nadeu F, Salmerón-Villalobos J, et al. Distinct molecular profile of IRF4-rearranged large B-cell lymphoma. Blood. 2020;135:274–86.
18. Schmitz R, Young RM, Ceribelli M, Jhavar S, Xiao W, Zhang M, et al. Burkitt lymphoma pathogenesis and therapeutic targets from structural and functional genomics. Nature. 2012;490:116–20.
19. Burkhardt B, Michgehl U, Rohde J, Erdmann T, Berning P, Reutter K, et al. Clinical relevance of molecular characteristics in Burkitt lymphoma differs according to age. Nat Commun. 2022;13:3881.
20. Thomas N, Dreval K, Gerhard DS, Hilton LK, Abramson JS, Ambinder RF, et al. Genetic subgroups inform on pathobiology in adult and pediatric Burkitt lymphoma. Blood. 2023;141:904–16.
21. Swerdlow S, Campo E, Harris N, Jaffe E, Pileri S, Stein H, et al., editors. WHO classification of tumours of haematopoietic and lymphoid tissues. 4th ed. Lyon: IARC; 2008.
22. Klapper W, Szczepanowski M, Burkhardt B, Berger H, Rosolowski M, Bentink S, et al. Molecular profiling of pediatric mature B-cell lymphoma treated in population-based prospective clinical trials. Blood. 2008;112:1374–81.
23. Hummel M, Bentink S, Berger H, Klapper W, Wessendorf S, Barth TFE, et al. A biologic definition of burkitt's lymphoma from transcriptional and genomic profiling. N Engl J Med. 2006;354:2419–30.
24. Dave SS, Fu K, Wright GW, Lam LT, Kluin P, Boerma EJ, et al. Molecular diagnosis of Burkitt's lymphoma. N Engl J Med. 2006;354:2431–42.
25. Woessmann W, Zimmermann M, Meinhardt A, Müller S, Hauch H, Knörr F, et al. Progressive or relapsed Burkitt lymphoma or leukemia in children and adolescents after BFM-type first-line therapy. Blood. 2020;135:1124–32.
26. Minard-Colin V, Aupérin A, Pillon M, Burke GAA, Barkauskas DA, Wheatley K, et al. Rituximab for high-risk, mature B-cell non-Hodgkin's lymphoma in children. N Engl J Med. 2020;382:2207–19.
27. Newman AM, Zaka M, Zhou P, Blain AE, Erhorn A, Barnard A, et al. Genomic abnormalities of TP53 define distinct risk groups of paediatric B-cell non-Hodgkin lymphoma. Leukemia. 2022;36:781–9.
28. Scholtysik R, Kreuz M, Klapper W, Burkhardt B, Feller AC, Hummel M, et al. Detection of genomic aberrations in molecularly defined Burkitt's lymphoma by array-based, high resolution, single nucleotide polymorphism analysis. Haematologica. 2010;95:2047–55.
29. Hans CP, Weisenburger DD, Greiner TC, Gascoyne RD, Delabie J, Ott G, et al. Confirmation of the molecular classification of diffuse large B-cell lymphoma by immunohistochemistry using a tissue microarray. Blood. 2004;103:275–82.
30. Colomo L, Vazquez I, Papaleo N, Espinet B, Ferrer A, Franco C, et al. LMO2-negative expression predicts the presence of MYC translocations in aggressive B-cell lymphomas. Am J Surg Pathol. 2017;41:877–86.
31. Vazquez I, Papaleo N, Lop J, Puiggros A, Sanchez-Gonzalez B, Diez-Feijoo R, et al. Lack of expression of LMO2 clone SP51 identifies MYC rearrangements in aggressive large B-cell lymphomas. Virchows Arch. 2021;479:1073–8.
32. Johnson NA, Slack GW, Savage KJ, Connors JM, Ben-Neriah S, Rogic S, et al. Concurrent expression of MYC and BCL2 in diffuse large B-cell lymphoma treated with rituximab plus cyclophosphamide, doxorubicin, vincristine, and prednisone. J Clin Oncol. 2012;30:3452–9.
33. Sureda-Gómez M, Iaccarino I, De Bolòs A, Meyer MA, Balsas P, Richter J, et al. SOX11 expression is restricted to EBV-negative Burkitt lymphoma and associates with molecular genetic features. Blood. 2024;144:187–200.
34. Cheung KJ, Rogic S, Ben-Neriah S, Boyle M, Connors JM, Gascoyne RD, et al. SNP analysis of minimally evolved t(14;18)(q32;q21)-positive follicular lymphomas reveals a common copy-neutral loss of heterozygosity pattern. Cytogenet Genome Res. 2012;136:38–43.
35. Wlodarska I, Stul M, De Wolf-Peeters C, Hagemeijer A. Heterogeneity of BCL6 rearrangements in nodular lymphocyte predominant Hodgkin's lymphoma. Haematologica. 2004;89:965–72.
36. Joos S, Falk MH, Lichter P, Haluska FG, Henglein B, Lenoir GM, et al. Variable breakpoints in Burkitt lymphoma cells with chromosomal t(8;14) translocation

separate c-myc and the IgH locus up to several hundred kb. Hum Mol Genet. 1992;1:625–32.
37. Hübschmann D, Kleinheinz K, Wagener R, Bernhart SH, López C, Toprak UH, et al. Mutational mechanisms shaping the coding and noncoding genome of germinal center derived B-cell lymphomas. Leukemia. 2021;35:2002–16.
38. Grande BM, Gerhard DS, Jiang A, Griner NB, Abramson JS, Alexander TB, et al. Genome-wide discovery of somatic coding and noncoding mutations in pediatric endemic and sporadic Burkitt lymphoma. Blood. 2019;133:1313–24.
39. Muppidi JR, Schmitz R, Green JA, Xiao W, Larsen AB, Braun SE, et al. Loss of signalling via Gα13 in germinal centre B-cell-derived lymphoma. Nature. 2014;516:254–8.
40. Lenz G, Davis RE, Ngo VN, Lam L, George TC, Wright GW, et al. Oncogenic CARD11 mutations in human diffuse large B cell lymphoma. Science. 2008;319:1676–9.
41. Mansouri L, Thorvaldsdottir B, Sutton LA, Karakatsoulis G, Meggendorfer M, Parker H, et al. Different prognostic impact of recurrent gene mutations in chronic lymphocytic leukemia depending on IGHV gene somatic hypermutation status: a study by ERIC in HARMONY. Leukemia. 2023;37:339–47.
42. Karube K, Enjuanes A, Dlouhy I, Jares P, Martin-Garcia D, Nadeu F, et al. Integrating genomic alterations in diffuse large B-cell lymphoma identifies new relevant pathways and potential therapeutic targets. Leukemia. 2018;32:675–84.
43. Schmitz R, Wright GW, Huang DW, Johnson CA, Phelan JD, Wang JQ, et al. Genetics and pathogenesis of diffuse large B-cell lymphoma. N Engl J Med. 2018;378:1396–407.
44. Chapuy B, Stewart C, Dunford AJ, Kim J, Kamburov A, Redd RA, et al. Molecular subtypes of diffuse large B cell lymphoma are associated with distinct pathogenic mechanisms and outcomes. Nat Med. 2018;24:679–90.
45. Wright GW, Huang DW, Phelan JD, Coulibaly ZA, Roulland S, Young RM, et al. A probabilistic classification tool for genetic subtypes of diffuse large B cell lymphoma with therapeutic implications. Cancer Cell. 2020;37:551–68.
46. Klapper W, Kreuz M, Kohler CW, Burkhardt B, Szczepanowski M, Salaverria I, et al. Patient age at diagnosis is associated with the molecular characteristics of diffuse large B-cell lymphoma. Blood. 2012;119:1882–7.
47. Richter J, John K, Staiger AM, Rosenwald A, Kurz K, Michgehl U, et al. Epstein–Barr virus status of sporadic Burkitt lymphoma is associated with patient age and mutational features. Br J Haematol. 2022;196:681–9.
48. Wästerlid T, Nordström L, Freiburghaus C, Pedersen M, Nørgaard P, Gang AO, et al. Frequency and clinical implications of SOX11 expression in Burkitt lymphoma. Leuk Lymphoma. 2017;58:1760–3.
49. López C, Kleinheinz K, Aukema SM, Rohde M, Bernhart SH, Hübschmann D, et al. Genomic and transcriptomic changes complement each other in the pathogenesis of sporadic Burkitt lymphoma. Nat Commun. 2019;10:1459.
50. Hilton LK, Collinge BJ, Ben-Neriah S, Alduaij W, Shaalan H, Weng A, et al. Motive and opportunity: MYC rearrangements in high-grade B-cell lymphoma with MYC and BCL2 rearrangements-an LLMPP study. Blood. 2024;144:525–540.
51. López C, Burkhardt B, Chan JKC, Leoncini L, Mbulaiteye SM, Ogwang MD, et al. Burkitt lymphoma. Nat Rev Dis Prim. 2022;8:78.
52. Szczepanowski M, Lange J, Kohler CW, Masque-Soler N, Zimmermann M, Aukema SM, et al. Cell-of-origin classification by gene expression and MYC-rearrangements in diffuse large B-cell lymphoma of children and adolescents. Br J Haematol. 2017;179:116–9.
53. Salaverria I, Martin-Guerrero I, Wagener R, Kreuz M, Kohler CW, Richter J, et al. A recurrent 11q aberration pattern characterizes a subset of MYC-negative high-grade B-cell lymphomas resembling Burkitt lymphoma. Blood. 2014;123:1187–98.
54. Shestakova A, Shao L, Smith LB, Ryan R, Bedell V, Murata-Collins J, et al. High-grade B-cell lymphoma with concurrent MYC rearrangement and 11q aberrations: clinicopathologic, cytogenetic, and molecular characterization of 4 cases. Hum Pathol. 2023;136:34–43.
55. Grygalewicz B, Woroniecka R, Rymkiewicz G, Rygier J, Borkowska K, Kotyl A, et al. The 11q-gain/loss aberration occurs recurrently in MYC-negative Burkitt-like Lymphoma With 11q Aberration, as well as MYC-positive Burkitt lymphoma and MYC-positive high-grade B-cell lymphoma, NOS. Am J Clin Pathol. 2018;149:17–28.
56. Havelange V, Ameye G, Théate I, Callet-Bauchu E, Lippert E, Luquet I, et al. The peculiar 11q-gain/loss aberration reported in a subset of MYC-negative high-grade B-cell lymphomas can also occur in a MYC-rearranged lymphoma. Cancer Genet. 2016;209:117–8.
57. Gonzalez-Farre B, Ramis-Zaldivar JE, Salmeron-Villalobos J, Balagué O, Celis V, Verdu-Amoros J, et al. Burkitt-like lymphoma with 11q aberration: a germinal center-derived lymphoma genetically unrelated to Burkitt lymphoma. Haematologica. 2019;104:1822–9.

ACKNOWLEDGEMENTS

We thank the centers of the Sociedad Española de Hematología y Oncología Pediátricas (SEHOP) that submitted cases for consultation and to Melika Bashiri, Laura Pla, Montse Sanchez, and Helena Suarez for their excellent technical assistance. We are indebted to the IDIBAPS Genomics Core Facility and to HCB-IDIBAPS Biobank-Tumor Bank and Biobanc de l'Hospital Infantil Sant Joan de Déu, Hospital Universitario Virgen del Rocío-Instituto de Biomedicina de Sevilla Biobank (ISCIII-Red de Biobancos PT13/0010/0056) all three integrated in the National Network Biobanks of ISCIII for the sample and data procurement.

AUTHOR CONTRIBUTIONS

SM performed research, analyzed data, and wrote the manuscript; NCdA reviewed and interpreted pathological data, analyzed data, and wrote the manuscript; AC performed research, analyzed data, and wrote the manuscript. LC, JSV, JERZ, FN, and NG performed research and analyzed data. LW reviewed and interpreted pathological data. JVA, MA, NC, VC, MJO, AG, IA, VPA, and EQ reviewed and interpreted clinical data. AJ and DWS performed research. EC reviewed and interpreted pathological data and wrote the manuscript. OB designed research, performed pathological diagnosis, analyzed data, and wrote the manuscript. IS designed and performed research, analyzed data, and wrote the manuscript.

FUNDING

This work was supported by Asociación Española Contra el Cáncer (PRYGN21911-SALA), Fondo de Investigaciones Sanitarias Instituto de Salud Carlos III (PI18/00471, PI21/00479) to IS, and PID2021-123054OB-I00 funded by MCIN/AEI/10.13039/501100011033 to EC and, as appropriate, by "ERDF A way of making Europe". Furthermore, the authors would like to thank the support of the Generalitat de Catalunya Support Grups de Recerca (2017-SGR-1107 and 2021-SGR-01293 to IS and 2021-SGR-01172 to EC). IS was supported by Miguel Servet II ISCIII (MS18/00015). SM holds a PFIS ISCIII fellowship (FI22/00063), AC holds an Investigo contract from Generalitat de Catalunya (100028TC7) and NG was supported by Acció instrumental d'incorporació de científics i tecnòlegs PERIS 2020 (SL017/20/000204) from Generalitat de Catalunya. EC is an Academia Researcher of the "Institució Catalana de Recerca i Estudis Avançats" (ICREA) of the Generalitat de Catalunya. DWS is supported by a Michael Smith Foundation Research, Health Professional Investigator Award. This work was developed at the Centro Esther Koplowitz, Barcelona, Spain.

COMPETING INTERESTS

The authors declare no competing interests.

ADDITIONAL INFORMATION

Supplementary information The online version contains supplementary material available at https://doi.org/10.1038/s41408-024-01153-0.

Correspondence and requests for materials should be addressed to Olga Balagué or Itziar Salaverria.

Reprints and permission information is available at http://www.nature.com/reprints

Publisher's note Springer Nature remains neutral with regard to jurisdictional claims in published maps and institutional affiliations.